Indian Journal of Pure & Applied Physics
Vol. 62, August 2024, pp. 642-655
DOI: 10.56042/ijpap.v62i8.10349

3D-Modelling and Analysis of All-Optical Carry Look-Ahead Adder Circuits using Nonlinear Structures

Sushanta Mahanty, Ajay Yadav & Ajay Kumar*
Department of Electronics and Communication Engineering, National Institute of Technology, Jamshedpur, Jharkhand 831 014, India

Received 11 April 2024; accepted 18 June 2024

This article proposes a high-speed secured data processing approach for an all-optical Carry Look Ahead (CLA) adder logic utilizing micro-ring resonators (MRRs). The proposed scheme facilitates high-speed arithmetic operations within the realm of all-optical nonlinear switching technology. The theoretical validation of this approach is demonstrated for a 4-bit CLA adder and is extendable to higher-order bits. Conventional methods of switching, computation, and data transmission often suffer from increased size, posing challenges in modern optical communication systems. To address the need for ultrafast switching, compact design, and reduced electromagnetic interference, the proposed approach leverages the innovative use of MRR as a switch, seamlessly integrating with a system in fiber (SIF). Designing the CLA adder in the all-optical domain using MRR, additional advantages are gained, such as minimizing propagation delay by computing the carry signal in advance, based on the fundamental concept of CLA adders. The optimal values of key constraints, including the ring radius and coupling coefficient, are thoroughly investigated, and the device parameters and performances are analysed. The proposed design of an all-optical CLA adder using MRR structure reinforces the theoretical foundation of the proposed scheme and has been replicated using MATLAB, accompanied by detailed mathematical descriptions, and subsequently verified.

Keywords: Micro ring resonator; Carry look ahead (CLA); System in fiber (SIF); All-optical circuit

1 Introduction

In recent years, the realization of ultrafast communication systems has become feasible with the advent of digitally computed optical outputs. Over the past few decades, numerous researchers have reported various digital logic circuits designed for optical domain applications, focusing not only on switching capabilities but also on aspects such as security, compact size, and reduced processing time. The performance of fiber-optic-based nonlinear switching and optical logic devices has been of particular interest, as they hold the potential to advance System in Fiber (SIF) technology, facilitating ultra-high-speed fiber communication systems for various networking applications. Research efforts have explored switching, routing, and data processing techniques compatible with fiber bandwidth, utilizing electro-optical conversion through devices such as Mach-Zehnder interferometers (MZI)[1–3]. Additionally, work has been conducted using semiconductor optical amplifiers (SOA) and MZI-SOA configurations[4–5]. Optical logic gates, arithmetic operations, code conversions, and sensing applications have been investigated utilizing MZI setups and directional couplers[6–8].

In the realm of ultra-fast optical computing, where photons play a crucial role in information transmission, the concept of all-optical switching controlled by light itself has gained prominence. Various optical switching circuits and devices have been developed for modern communication systems and information processing networks[9–13]. All-optical switching mechanisms involve inducing control pump signal light externally onto optical micro rings, enabling on/off conversion crucial for routing information in response to the optical control pump signal. The advancement of ultrafast all-optical transmission networks within System-in-Fiber (SIF) architectures promises significant progress in very large-scale integrated optics (VLSIO). Furthermore, optical switching schemes utilizing Micro-Ring Resonators (MRR) have been extensively explored for logic operations such as NAND, NOR, XOR, and arithmetic logic operations[14–16]. Researchers have developed different code conversion circuits compatible with optical bandwidth within the all-optical domain using MRR structures[17–20]. All-optical signal processing for memory devices such as flip-flops and complex sequential circuits, including sequence generators, detectors, and shift registers, has been demonstrated using MRR and

*Corresponding author: (E-mail: ajaynitjsr93@gmail.com)

Fiber Bragg Grating structures[21–25]. Silicon photonics emerges as a promising technology in contemporary trends, with MRRs being preferred for switching and sensing applications over other photonic devices like MZIs and Terahertz Optical Asymmetric De-multiplexers (TOADs)[26]. Researchers are recently reported some logical circuits for ultra-fast devices for data transmission in modern scenario of communication system[27-32].

This paper focuses on the theoretical description and validation of an all-optical Carry Look-Ahead (CLA) adder designed for high-speed data processing using MRR structures. Section 1 presents the proposed CLA adder's operation theoretically, validated with conventional truth tables. Section 2 provides an overview of the basic concept of the CLA adder, followed by an exploration of using MRR structures as influential optical switching schemes. The thorough examination of device parameters demonstrates the suitability of the proposed unit within the optical domain. Optimization of device parameters and key performance parameters are discussed in detail. Section 2 also addresses the layout of the suggested MRR switching-based all-optical CLA adder. Finally, this paper discusses how the selected device parameters yield the desired outcomes, confirmed through appropriate simulation results and mathematical modelling. The proposed approach overcomes inherent challenges associated with optical-to-electrical and electrical-to-optical conversions, offering a theoretically sound method for achieving optimal results with the ultrafast MRR-based CLA adder, leveraging the advantages of all-optical switching phenomena.

2 Micro-ring resonator based All-optical Carry Look Ahead adder

2.1 Introduction to Conventional CLA adder

In the realm of data transmission and information processing, the silicon photonics approach emerges as an efficient and promising solution for achieving secure, ultra-fast modern communication. Fulfilling the requirements of all-optical Carry Look-Ahead (CLA) adders become imperative in this context. The propagation time of any circuit stands out as a crucial characteristic of digital integrated circuits. During arithmetic operations such as addition, subtraction, multiplication, and division, carry signals are generated, with carry propagation time emerging as a significant concern. To facilitate high-speed data processing, reducing the carry propagation delay of adders emerges as a key strategy. Various logic and design methods are actively being researched to minimize this delay. By computing the carry signal in advance for all possible input combinations, we aim to minimize propagation delay, leveraging the fundamental concept of CLA adders. Specifically, when both input bits are 1, a carry is generated. Additionally, a carry is produced when one of the two bits is 1, and there is also a carry from the previous step.

Carry propagation time represents a critical speed-limiting factor for ripple carry adders. Furthermore, multiplication and division, which often involve multiple add/subtract steps, are arithmetic processes that are directly impacted by the speed of addition. Hence, minimizing the carry propagation latency of adders becomes essential to accelerate these arithmetic processes. Various logic design strategies have been employed to address the carry propagation problem. One common approach leverages the CLA principle to anticipate carry signals based on input signals, leading to the development of CLA adder circuits. CLA adders concurrently compute the carry-in for each complete adder by employing streamlined equations involving Pi, Gi, and Cin. This approach effectively reduces propagation time, as only the first carry signal sent at the input determines the output carry at any given step. Consequently, CLA adders stand out as the fastest adders when compared to other additive processes. The truth table of the CLA adder, depicted in Table 1 below, is the focus of our study, specifically targeting the design of a four-bit CLA adder in an isolated section.

Figure 1 illustrates the pictorial representation of a 4-bit CLA adder, showcasing the initial generation of carry signals and their simultaneous propagation to the subsequent stages for further arithmetic operations. This figure also illustrates how propagation delay can be minimized to achieve ultra-fast arithmetic operations, leading to optimized results.

Table 1 — Truth Table of CLA adder

A	B	Cin	SUM	CARRY	CONDITION
0	0	0	0	0	No Carry Occurs
0	0	1	1	0	
0	1	0	1	0	
0	1	1	0	1	Carry Propagation
1	0	0	1	0	No Carry
1	0	1	0	1	Carry Propagation
1	1	0	0	1	Carry Occurs
1	1	1	1	1	

Figure 2 presents the conventional logical circuit diagram of a CLA adder, where Carry Generation is denoted as (Gi) and Carry Propagation as (Pi). When an input carry is provided, the transmission of an output carry is observed. We use Pi as a reference in this context, which can be mathematically expressed as $Pi = Ai \oplus Bi$. Referring to the truth table, it's evident that an output carry is generated if both inputs, A and B, are high, irrespective of the input carry magnitude. This output carry is denoted as Gi, which can be mathematically expressed as $Gi = Ai * Bi$.

The initial equations for a complete adder are as follows: $Sum = A \oplus B \oplus Ci$ and $Carry = Ci(A + B) + AB$. Therefore, $Sum = Pi \oplus Ci$, and $Carry = Gi + Pi \cdot Ci$. These equations for the entire adder can be rewritten in terms of Pi and Gi.

The carry outputs, denoted as C0, C1, C2, and C3, are derived based on the equations provided above.

$$C_0 = (C_{in} . P_0) + G_0$$

$$C_1 = (C_{in} . P_0 . P_1) + (G_0 . P_1) + G_1$$

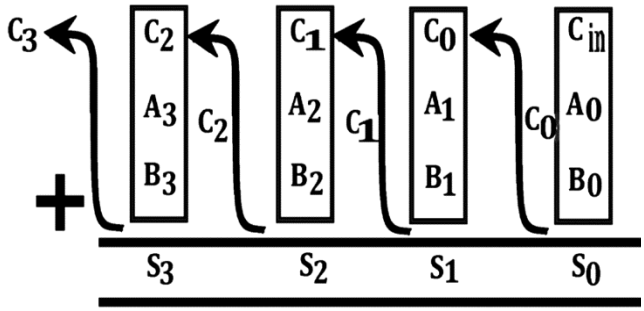

Fig. 1 — Basic Scheme of Carry Look Ahead adder

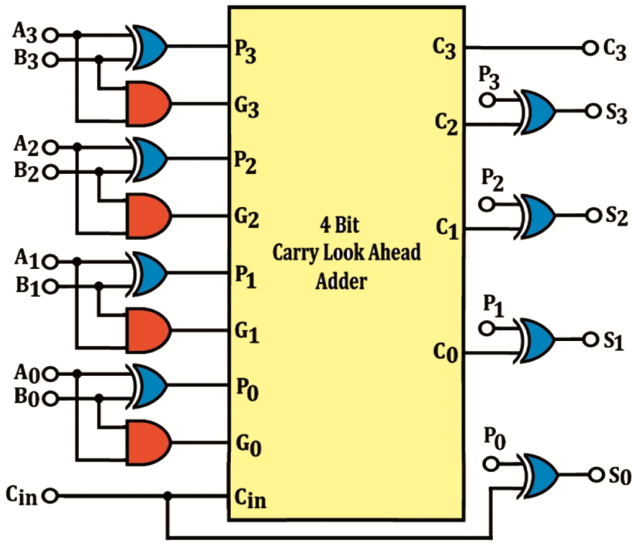

Fig. 2 — Circuit diagram of CLA adder

$$C_2 = G_2 + (P_2 . G_1) + (P_2 . P_1 . G_0) + (P_2 . P_1 . P_0 . C_{in})$$

$$C_3 = (C_{in} . P_0 . P_1 . P_2 . P_3) + (P_3 . P_2 . P_1 . G_0) + (P_3 . P_2 . G_1) + (G_2 . P_3) + G_3$$

Similarly, the sum outputs, denoted as S0, S1, S2, and S3, are calculated using the following equations: $S_0 = C_{in} \oplus P_0, S_1 = C_0 \oplus P_1, S_2 = C_1 \oplus P_2, S_3 = C_2 \oplus P_3$. These equations allow for the determination of the sum outputs S0, S1, S2, and S3 based on the input carry Cin and the carry and propagate signals P0, P1, P2, and P3.

2.2 The basic Switching operation of MRR Structure

The MRR stands as a fundamental component within the proposed solution, serving a pivotal role in optical signal processing systems. The functionality of an optical resonator relies on satisfying total internal reflection (TIR) conditions to confine light within the waveguides. The micro-ring resonator structure comprises a circular waveguide surrounded by straight waveguides, with coupling coefficients represented as k_1 for the input waveguide and k_2 for the output waveguide. These coefficients govern the coupling of the input and output waveguides to the ring waveguide through directional couplers.The phenomenon of "on-resonance" determines the transmission behavior at respective ports. Constructive interference of light is essential for successful resonance, where the circumference of the ring must be an integer multiple of the wavelength of light ($m\lambda = 2\pi R \cdot neff$), resulting in the appearance of bright fringes at the output port.

Figure 3 illustrates the structure of the micro-ring resonator, highlighting its configuration for optical

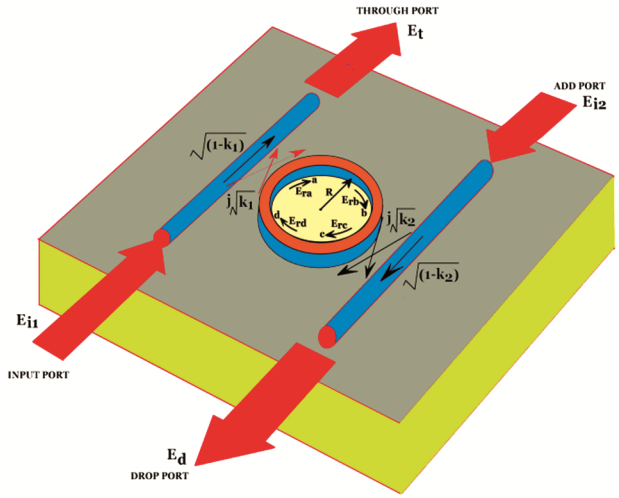

Fig. 3 — Micro-ring resonator structure

signal manipulation. A specific wavelength achieves resonance within the ring, which is regulated by a pump signal introduced via a laser. In the absence of pump power, the through port exhibits minimal transmittance, while reversing the signal maximizes transmittance at the drop port. The nonlinear material within the resonator induces a change in the refractive index, utilizing photons as carriers for high-speed data processing in the terahertz (THz) range. As the refractive index changes, a π-phase shift occurs within the ring, facilitating the switching of output light from one port to another due to the two-photon absorption (TPA) phenomenon, thus enabling the switching action. Considering the circumference $(2\pi R)$ of the ring as L, along with field coupling coefficients ($k_1$and k_2), intensity attenuation coefficients (α), intensity loss coefficients (γ), and the wave propagation constant (kp), where λ represents the resonant wavelength, the transmission characteristics at the Through Port (E_t) and the Drop Port (E_d)[17-19, 24,25].

$$E_t = \frac{D\sqrt{1-k_1} - D\sqrt{1-k_2}x^2exp^2(j\phi)}{1-\sqrt{1-k_1}\sqrt{1-k_2}x^2exp^2(j\phi)}E_{i1} + \frac{-D\sqrt{k_1k_2}x\,exp(j\phi)}{1-\sqrt{1-k_1}\sqrt{1-k_2}x^2exp^2(j\phi)}E_{i2} \quad \ldots (1)$$

$$E_d = \frac{-D\sqrt{k_1k_2}x\exp(j\phi)}{1-\sqrt{1-k_1}\sqrt{1-k_2}x^2exp^2(j\phi)}E_{i1} + \frac{D\sqrt{1-k_1} - D\sqrt{1-k_2}x^2exp^2(j\phi)}{1-\sqrt{1-k_1}\sqrt{1-k_2}x^2exp^2(j\phi)}E_{i2} \quad \ldots (2)$$

The general equations E_t and E_d represent the main terms for switching activity in ring resonators, aiding diverse design and analysis for any combinational and sequential logic circuits. Fig. 4 shows the switching behaviour in the MRR structure under various control signal circumstances, specifically the transition from low to high transmittance states at the output ports.

Figure 5(a & b) illustrate the simulation results and switching principle of the single MRR structure, respectively. In Fig. 5(a), the 3-D simulation results show the propagation of the normalized optical pulse within the single MRR structure. The pulse propagation demonstrates switching behaviour in response to the optical control pulse signal. Specifically, the normalized optical pulse is observed at the DP in the absence of the control pump signal, while it propagates through the TP in the presence of the optical control pump signal. In Fig. 5(b), the switching principle of the MRR structure is visualized using software simulation. The diagram illustrates how the control signal, initiated by a green laser, triggers the switching action. Output is generated at the TP in the presence of the pump signal, whereas the signal is received at the DP in its absence.

Figure 6 demonstrates the transfer function and the temporary blue shift of a single MRR structure with seamless switching action at TP and DP appearing in corresponding ports.

Figure 7 shows the Deviation of Phase Shift with average pump power in MRR structure. The refractive index variation (Δn) involved in the transfer function analysis is represented by Eq. 3:

$$\Delta n = -\left[8.8\times10^{-22}\frac{\beta t_p^2}{2h\upsilon\sqrt{\pi}S^2}P_{avg}^2 + 8.5\times10^{-22}\left(\frac{\beta t_p^2}{2h\upsilon\sqrt{\pi}S^2}P_{avg}^2\right)^{0.8}\right] \quad \ldots (3)$$

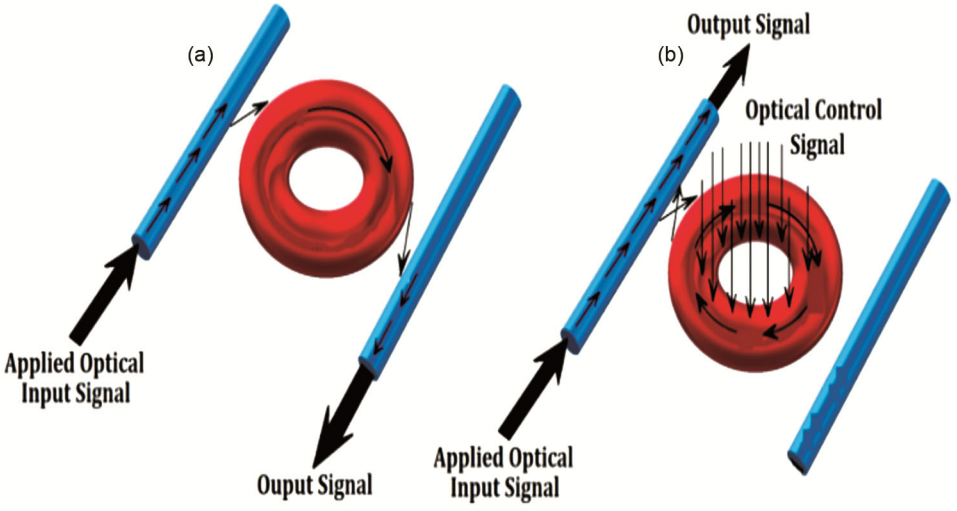

Fig. 4 — Switching performance in All-optical MRR structure (a) withoutpump signal (b) with the pump signal

The approach to proper blue shifting occurrences at the specified optical window is delivered by the mathematical Eqs 1-3. Due to the refractive index variation Δn and is illustrated in Eq. 4:

$$\phi = \left[\frac{2\pi}{\lambda}\right]\Delta nL \quad \ldots (4)$$

The MATLAB simulation results, as shown in Fig. 6, enable the observation of the phase shift corresponding to different wavelengths. Additionally, Fig. 7 illustrates the phase shift deviations with average pump power. According to the waveform, it is suggested that for π phase shift the required pump power of 2.552 mW.

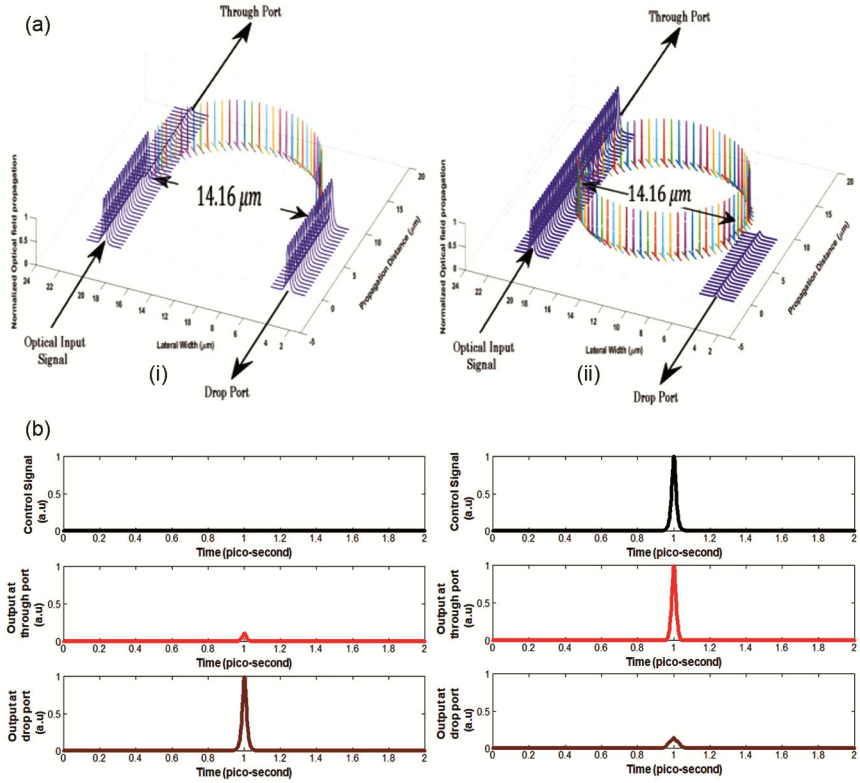

Fig. 5 — (a) MATLAB simulation results illustrate the normalized optical field propagation in the single MRR structure under two conditions: (i) In absence of the pump signal and (ii) In presence of the pump signal. (b) Simulated waveforms of switching performance of MRR structure

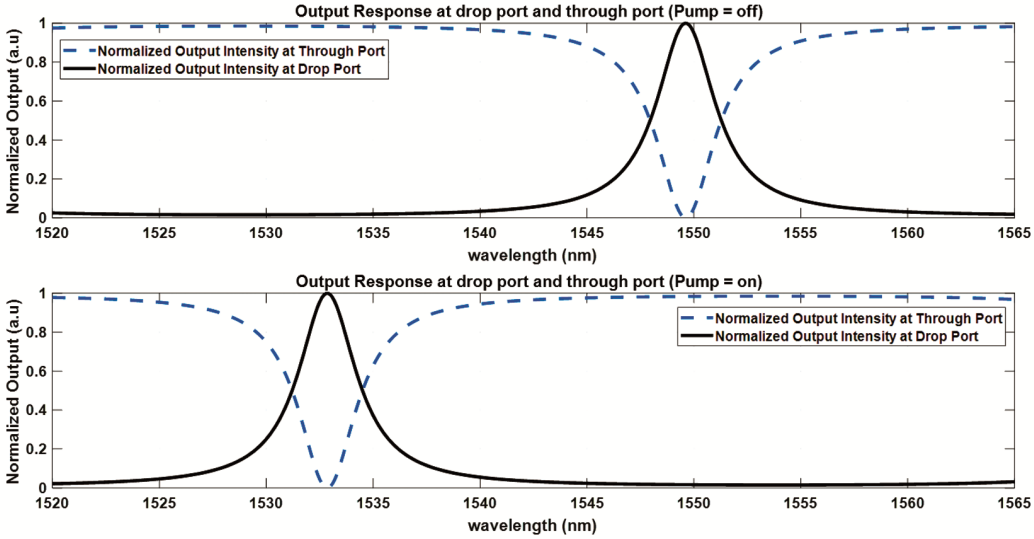

Fig. 6 — Specified wavelengths of 1550nm in presences of pump signal and absence of pump signal the Transfer function of normalized output response at the TP and DP

2.3 Analysis of radius and coupling coefficients of Single MRR Structure

The coupling coefficients k_1 and k_2 play crucial roles in enabling successful optical switching within MRR. In the absence of a control signal sent to the ring resonator, the optical signal emerges at the MRR's drop port. Conversely, when an optical pumping signal is applied vertically from the top of the ring, an optical signal is observed at the MRR's through port. Leveraging this phenomenon, MRRs are utilized to achieve optical switching activity, with the ideal values of k_1 and k_2 being essential for achieving appropriate MRR switching. The findings are illustrated in Figs 8 & 9, respectively, demonstrating how different combinations of these coupling coefficients were employed to obtain the ideal values for k_1 and k_2.

Additionally, the radius of the resonator plays a substantial role in the switching activity of MRR structure. By selecting an appropriate value, optimized output can be obtained. we found that an optimum value of radius $R = 7.089\ \mu m$ yields the desired performance.

Data Rate

The data rate or speed of operation of the micro-ring resonator circuit can be obtained from the relation given in Eq. 5[24]:

$$T = \frac{Y^2}{1 + X^2 - 2X\cos\emptyset} \quad \ldots (5)$$

Where $= \cos^2(k) \exp\left(-\alpha\pi R\right), Y = \sin^2(k) \exp(-\alpha\pi R/2)$, and $\emptyset = n_{eff}\frac{4\pi R^2}{\lambda}$

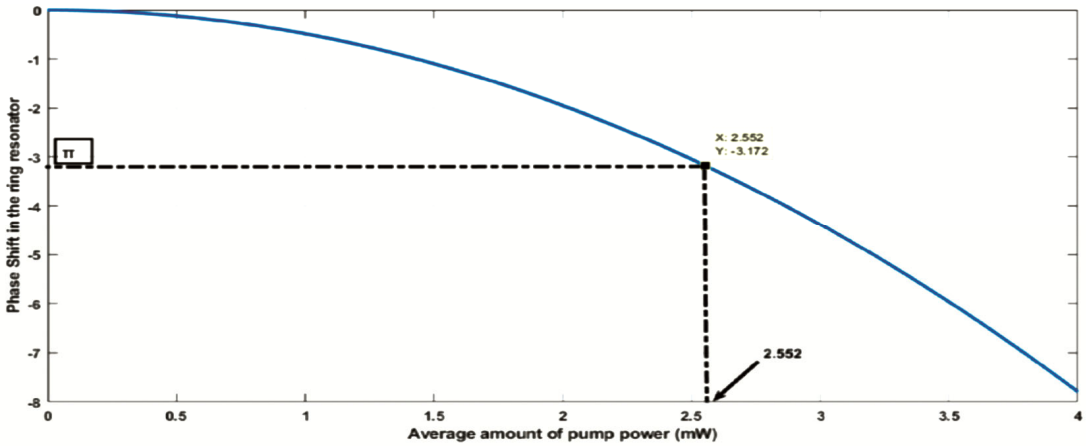

Fig. 7 — Deviation of Phase Shift with average pump power in MRR structure

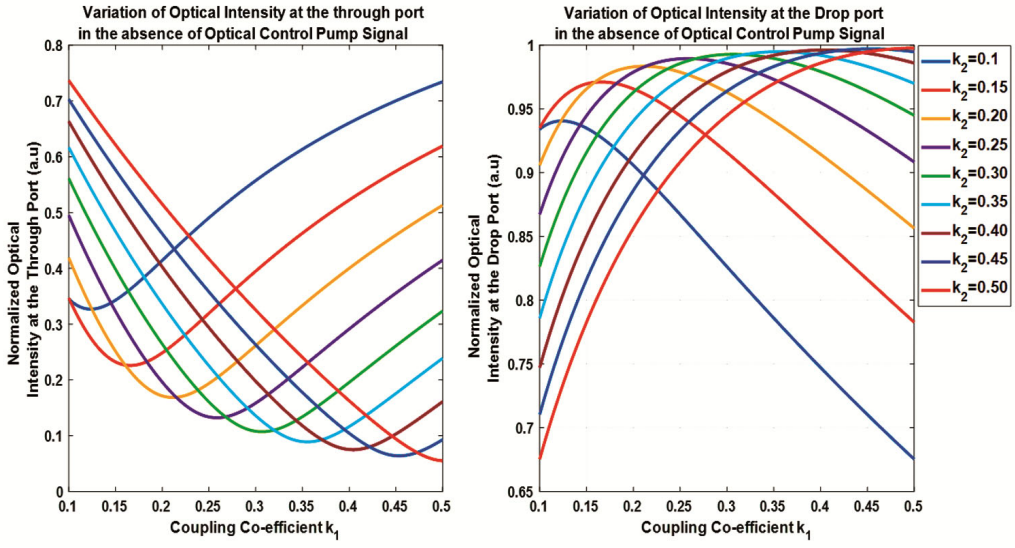

Fig. 8 — Intensity fluctuation at the TP and DP with varying values of k_1 when k_2 ranges from 0.1 to 0.5 in the absence of a pump signal

The response time of the proposed structure of MRR estimated at 100 Gbps. for committing high speed communication systems in optical domain nonlinear photonics, it is decisive that the rate of data processing and ER are extremely high and the propagation time is low. In comparison to other optical switching methods, MRR-based switching offers the highest value. Additionally, MRR-based switching has the lowest propagation time, approximately 2.52 ps, compared to other switching techniques.

2.4 Design of All-optical Carry Look Ahead adder using cascaded micro ring structure

The layout diagram of the all-optical CLA adder employs 30 identical MRRs to illustrate the precise switching occurrences associated with the all-optical CLA adder. In Fig. 10, MRR1, MRR2, and MRR3 are utilized to generate G_0 and. P_0 Specifically, G_0 is obtained through an AND operation $(G_0 = A_0.B_0)$ using MRR1 and MRR2, while P_0 is the result of an XOR operation $(P_0 = A_0 \oplus B_0)$ using MRR1 and MRR3. Similarly, MRR4, MRR5, and MRR6 produce

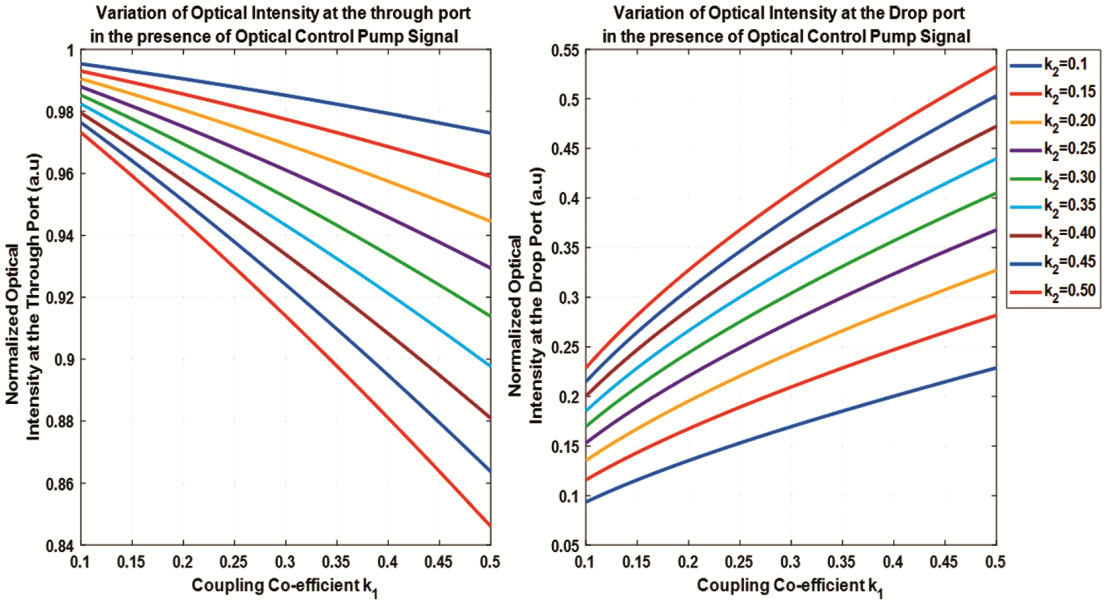

Fig. 9 — Intensity fluctuation at the TP and DP with varying values of k_1 when k_2 ranges from $0.1 - 0.5$, in the presence of a pump signal

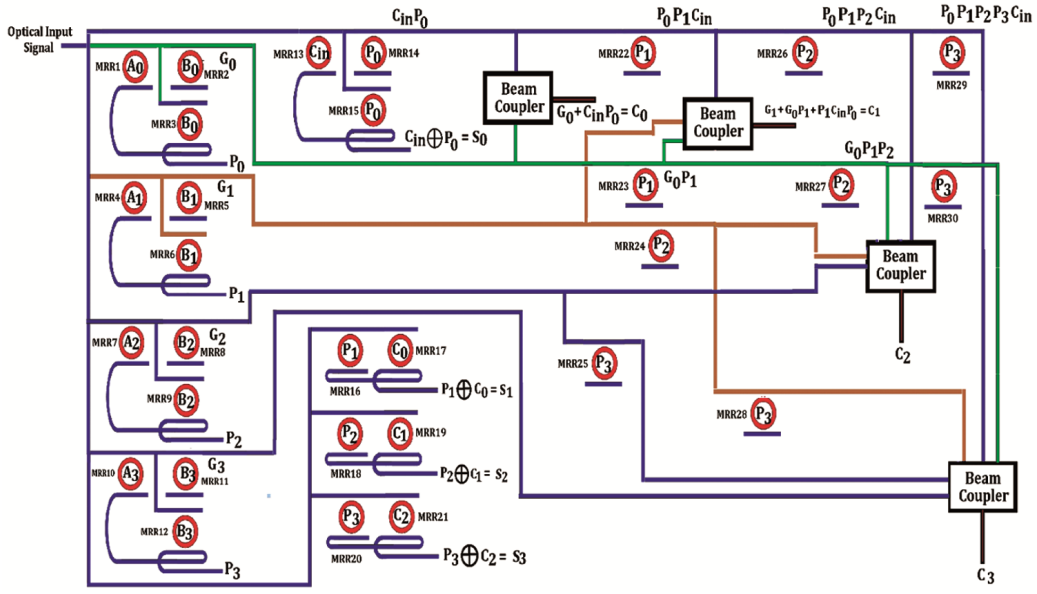

Fig. 10 — Schematic layout of All-optical CLA adder using cascaded MRR structure

G_1 and P_1 in terms of A_1 and B_1, where $G_1 = A_1.B_1$ and $P_1 = A_1 \oplus B_1$. Further more, MRR7, MRR8, and MRR9 generate G_2 and P_2 in terms of $A_2 and B_2$, with $G_2 = A_2.B_2$ and $P_2 = A_2 \oplus B_2$. Finally, MRR10, MRR11, and MRR12 produce G_3 and P_3 in terms of A_3 and B_3, where $G_3 = A_3.B_3$ and $P_3 = A_3 \oplus B_3$. For the output sum S_0, MRR13, MRR14, and MRR15 perform an XOR operation of Cin and P_0, where the carry-in (Cin) is active LOW. The corresponding carry output C_0 is produced with the help of a beam coupler. C_1 is generated using the output of MRR22 and MRR23, and G_1 is coupled through a beam coupler. Similarly, C_2 is generated using MRR26 and MRR27, and G_2 is coupled with a beam coupler. Finally, C_3 is collected using MRR25, MRR28, MRR29, and MRR30 along with G_3 with the help of a beam coupler. The sum output of the CLA adder, S_1, is observed as the XOR operation of P_1 and C_0 using MRR16 and MRR17. S_2 is obtained as the XOR operation of P_2 and C_1 using MRR18 and MRR19, and S_3 is observed as the XOR operation of P_3 and C_2 using MRR20 and MRR21, respectively. The outputs of the first stages, P_0, P_1, P_2, and P_3, serve as pumping power signals for the subsequent stages, necessitating a proper switching mechanism as per the desired routing of the input signal. Similarly, C_0, C_1, andC_2 are also required as pumping signals for producing the sum outputs S_1, S_2, and S_3.

Figure 11(a) illustrates the MATLAB 3-D simulation results of the proposed CLA adder structures, considering single MRR pulse propagation as a basic module. It is evident that the optical input signal is applied to the input port of MRR (1, 4, 7, 10, 13, 16, 18, and 20). The 3-D simulation of optical pulse propagation has been conducted for the input combination $A_3A_2A_1A_0 \rightarrow 0111$ & $B_3B_2B_1B_0 \rightarrow 0111$, with $C_{IN} \rightarrow 0$. The specific arrangement of MRR1-MRR3 demonstrates the propagation of the pulse in a manner where G_0 behaves as logic HIGH, while P_0 (Drop port of MRR3) exhibits the absence of a pulse. Similarly, the specific configuration of MRR4-MRR6 switches the pulse to obtain $G_1 \rightarrow$ HIGH, $P_1 \rightarrow$ LOW. Furthermore, switching of the pulse can be observed as $G_2 \rightarrow$ HIGH, $P_2 \rightarrow$ LOW, $G_3 \rightarrow$ LOW and $P_3 \rightarrow$ LOW. Now, the status of P_0 and C_{IN} serves as the optical control pump signal for the set of MRR13-MRR15, resulting in $S_0 =$ LOW. Similarly, MRR16 and MRR17 can be operated by the control pump signal P_1 and C_0 respectively, providing the signal S_1 as HIGH. Wherein, C_0 is derived from G_0, P_0, and C_{IN}, i.e., active LOW. Similarly, C_1, C_2, andC_3, the specific configuration of MRR, are connected in a manner to produce the desired output and verify the conventional truth table.Figure 11(b) depicts the time domain results of the proposed all-optical CLA adder simulation using MATLAB. In the first row, $C_{IN} \rightarrow 0$ is clearly displayed, indicating a LOW state. The second row of Fig. 11(b) illustrates the 4-bit input combination, while the third row represents another input, $B_3B_2B_1B_0 \rightarrow 0111$. The sum and carry outputs of the specified input combination are shown in the fourth and fifth rows, respectively, with the corresponding outputs verified against the conventional truth table.

Figure 12(a) presents the MATLAB 3-D simulation results of the proposed CLA adder structures, utilizing single MRR pulse propagation as a fundamental module. In the simulation, optical input signals are applied to the input ports of MRRs (1, 4, 7, 10, 13, 16, 18, and 20). The 3-D simulation evaluates the optical

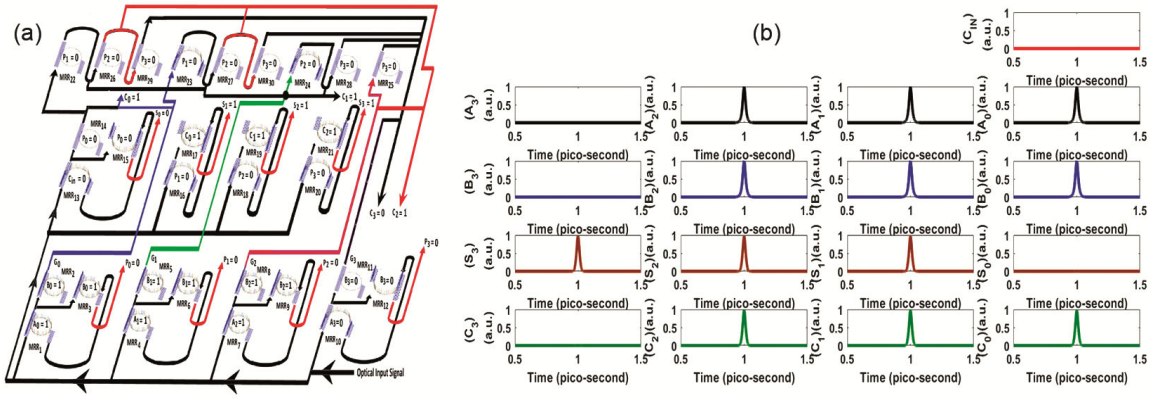

Fig. 11 (a) — Simulated Results of the proposed model of All-Optical CLA adder, representing the 3D Normalized Optical Pulse propagation, for the Input Bit Combination $A_3A_2A_1A_0 \rightarrow 0111$ & $B_3B_2B_1B_0 \rightarrow 0111$ & $C_{IN} \rightarrow 0$. (b) Results of the suggested all-optical CLA adder simulation, where Input sequences are $A_3A_2A_1A_0 \rightarrow 0111$ & $B_3B_2B_1B_0 \rightarrow 0111$ & $C_{IN} \rightarrow 0$

pulse propagation for the input combination $A_3A_2A_1A_0 \rightarrow 1011$, $B_3B_2B_1B_0 \rightarrow 0011$, and $C_{IN} \rightarrow 0$. Specifically, the arrangement of MRR1-MRR3 demonstrates the propagation of pulses such that G_0 exhibits a logic HIGH, while P_0 (Drop port of MRR3) shows the absence of a pulse. Similarly, the configuration of MRR4-MRR6 switches the pulse to achieve $G_1 \rightarrow$ HIGH and $P_1 \rightarrow$ LOW. This pattern continues with $G_2 \rightarrow$ LOW, $P_2 \rightarrow$ LOW, $G_3 \rightarrow$ LOW and $P_3 \rightarrow$ HIGH. The status of P_0 and C_{IN} functions as the optical control pump signal for MRR13-MRR15, resulting in $S_0 = LOW$. Likewise, MRR16 and MRR17 operate with the control pump signal $P\_1 \text{and} C\_0$ respectively, yielding S_1 as HIGH. C_0 is derived from $G_0, P_0,$ and C_{IN}, *i.e.*, active LOW. Similarly, the configurations of MRRs for $C_1, C_2,$ and C_3, are interconnected to produce the desired output and validate the conventional truth table.

The simulated time domain results of Fig. 12(b) illustrate the proposed all-optical CLA adder. In the second row, the input sequences $A_3A_2A_1A_0 \rightarrow 1011$ and $B_3B_2B_1B_0 \rightarrow 0011$ are reflected, while the corresponding sum output is obtained in the fourth row, and the carry outputs are shown in the fifth row. The first row of the waveform represents $C_{IN} \rightarrow 0$. The conventional output of the CLA adder is satisfied and verified with the proposed all-optical CLA adders.

2.5 Analysis of performance-affecting parameters in the proposed unit

In a single MRR structure, two critical factors include the coupling coefficients (K_1 and K_2) and the ring radius R. To ensure proper switching, these factors are investigated thoroughly. Through the proposed switching mechanism utilizing MRR, verified simulated waveforms are obtained at the optimal values of $k_1 = k_2 = 0.25$ and $R = 7.089\ \mu m$, which are explored in detail for the proposed layout of the 4-bit CLA adder. Fig. 13 depicts the variation in output intensities for the wavelength of the input CW signal within a specific optical window at both the through port (TP) and drop port (DP) of the MRR structure, for the both in presence and absence of a pump signal.

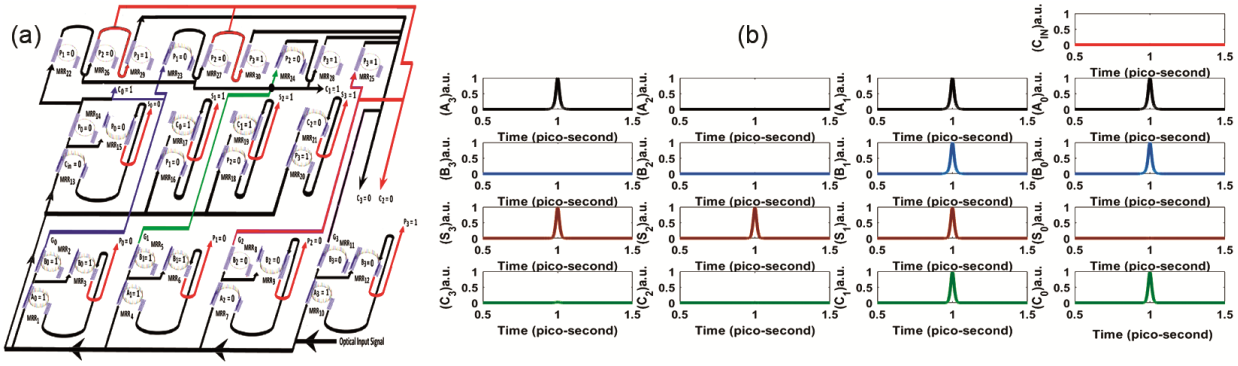

Fig. 12 (a) — Simulated Results of the proposed model of All-Optical CLA adder, representing the 3D Normalized Optical Pulse propagation, for the Input Bit Combination $A_3A_2A_1A_0 \rightarrow 1011$ and $B_3B_2B_1B_0 \rightarrow 0011$ and $C_{IN} \rightarrow 0$. (b) Results of the suggested all-optical CLA adder simulation, where Input sequences are $A_3A_2A_1A_0 \rightarrow 1011$ & $B_3B_2B_1B_0 \rightarrow 0011$ and $C_{IN} \rightarrow 0$

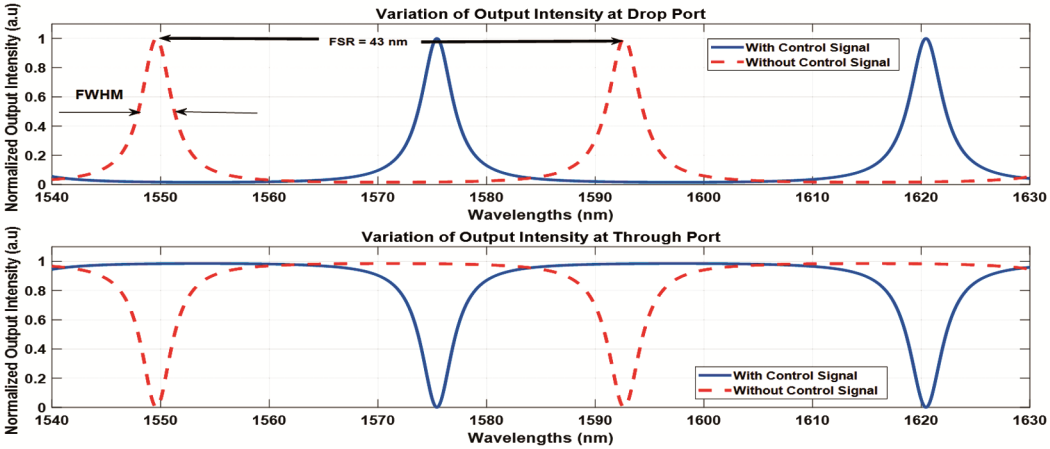

Fig. 13 — P and DP intensity variations with pump signal and without pump signal

Extinction ratio (ER)

The ER can be mathematically expressed as[22,24],

$$ER(dB) = 10.log\left(\frac{P^1_{min}}{P^0_{max}}\right) \quad \ldots (6)$$

Where $P^1_{min}$the min value of the peak intensity and $P^0_{max}$is the maxvalue of the peak intensity.

The variation of ER due to coupling coefficients and radius is depicted in Figs 14 & 15, respectively. In the performance analysis of the proposed layout structure of the 4-bit CLA adder, Fig. 10 illustrates some of the observed outputs, such as S_0, S_1, S_2 and C_3. In Fig. 14, the highest ER values are observed at $18.99\,dB$ for $S_0, S_1,$ and S_2, while the extinction ratio for output C_3 is $18.25\,dB$ when the coupling coefficients are set to $k_1 = k_2 = 0.25$. Fig. 15 displays the change in ER concerning the ring radius R. The highest ER value is $19.21\,dB$, and the minimum value is $18.98\,dB$ at the C_3 output port when the ring radius is $7.089\,\mu m$. Since C_3 is obtained after passing through more stages, its performance parameters are slightly poorer compared to S_0 to S_3. However, optimal parameters such as radius and coupling coefficients provide the most acceptable values of performance parameters, as indicated in these two graphs. Consequently, we conclude that the selected optimal values of k1 = k2 and the ring radius R are suitable for achieving the desired performance.

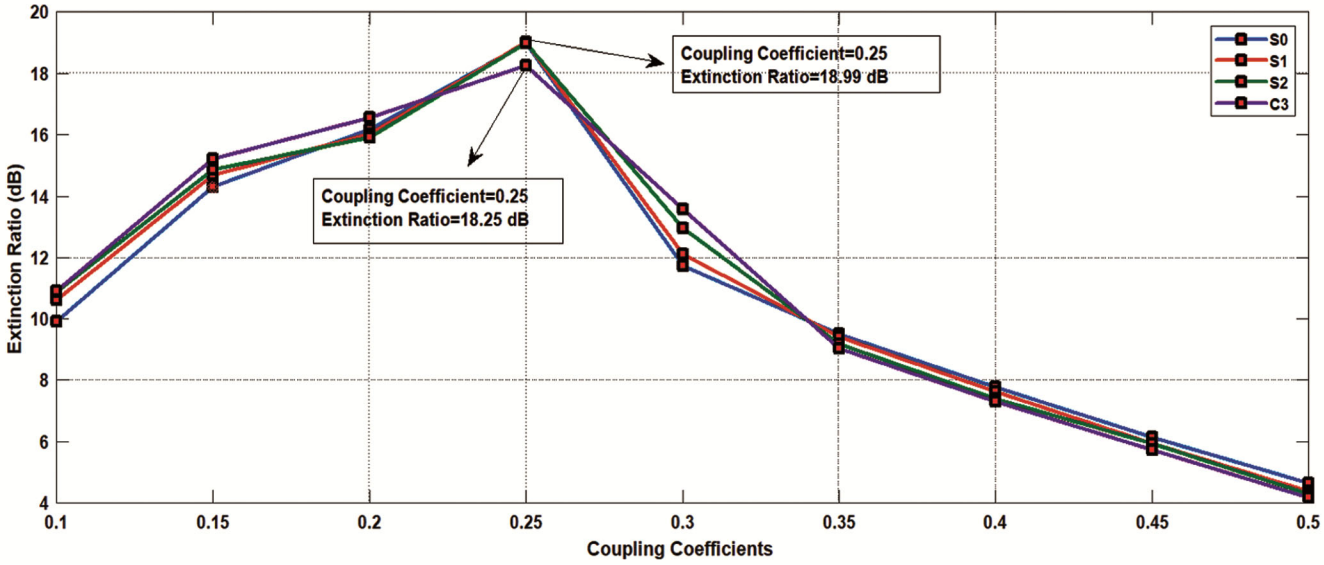

Fig. 14 — Extinction Ratio Variation with Various Values of Coupling Coefficients

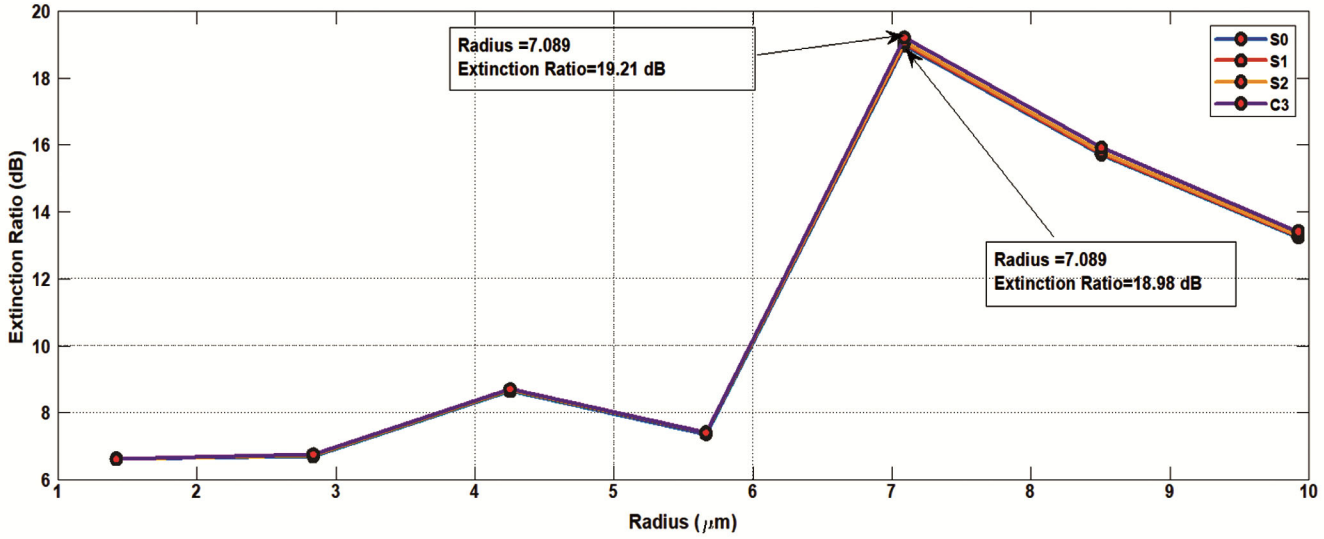

Fig. 15 — Extinction Ratio Variation with Different Radius of the ring resonator

Contrast ratio (CR)

The contrast ratio (CR) of the outputs is well-defined between the ratio of two one is the mean value of output intensity and another is the mean output intensity given as[24],

$$CR(dB) = 10log\left(\frac{P^1_{mean}}{P^0_{mean}}\right) \quad \ldots (7)$$

For optimal results, the CR should be as high as possible for the maximum portion of input that can appear at the output port.

Figures 16 & 17 illustrate the change in contrast ratio concerning variations in coupling coefficient and ring radius, respectively. In Fig. 16, it is observed that for coupling coefficients set to 0.25, the highest CR value reaches $20.24\,dB$. Conversely, Fig. 17 demonstrates that with a radius of $7.089\ \mu m$, the maximum value of CR is $19.68\,dB$.

Amplitude modulation (AM)

The ring resonator having AM can be defined as[24]

$$\mathrm{AM(dB)} = 10\log\left(\frac{\mathrm{P^1_{max}}}{\mathrm{P^1_{min}}}\right) \quad \ldots (8)$$

Where $\mathrm{P^1_{max}}$ and $\mathrm{P^1_{min}}$ are the max value and min values of intensity at a high (1) level. The value of AM should be less than 1dB[24]. Figures 18 & 19 present the patterns generated to determine the optimal AM value. In Fig. 18, the influence of coupling coefficient variation on AM is depicted, revealing that the minimum AM magnitude, recorded

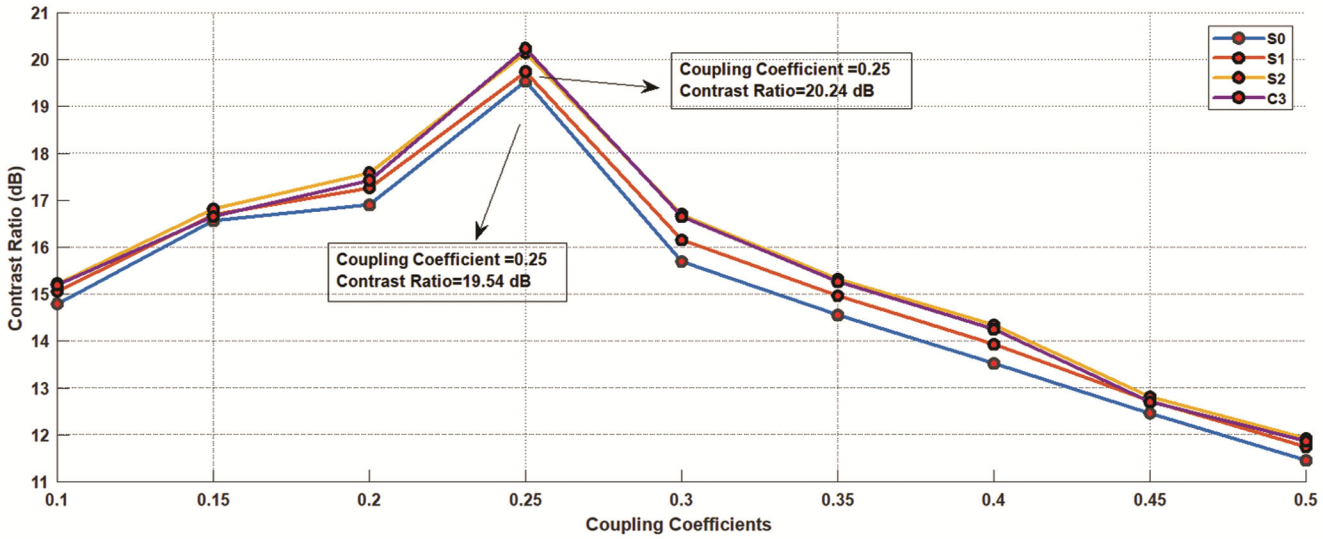

Fig. 16 — Variations in CR with Different values of the Coupling Coefficient

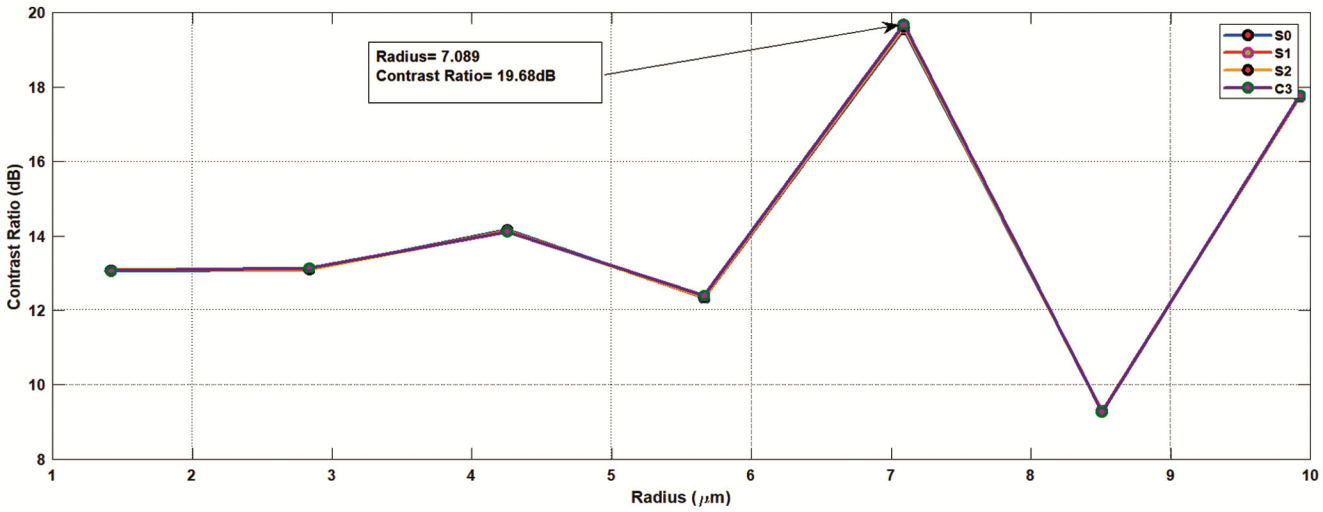

Fig. 17 — Variations in CR withDifferentradius of the ring resonator

at a coupling coefficient of 0.25, is $0.01006\,dB$ for various output configurations of the proposed setup. This outcome highlights the appropriateness of our selection for the coupling coefficient value. Fig. 19 demonstrates the outcome of altering the ring radius (R) on AM, indicating that a radius of $7.089\ \mu m$ results in the lowest AM value recorded at $0.01643\ dB$.

Switching speed

In a MRR, rapid transitions between the states of the output optical signal are facilitated by employing a CW optical input signal along with a pump signal. This setup leads to the observation of exceptionally quick rising and falling edges in the output signal. When the CW signal is introduced to the ring waveguide of the resonator along with the pump signal, the output signal experiences an increase, while it decreases to a low level when the pump signal is removed. The rise and fall times of the MRR are illustrated in Fig. 20(a & b).

The switching time, indicated by the rise time 2.531 and fall time of 2.52 picoseconds, is clearly depicted in Fig. 20(a & b).

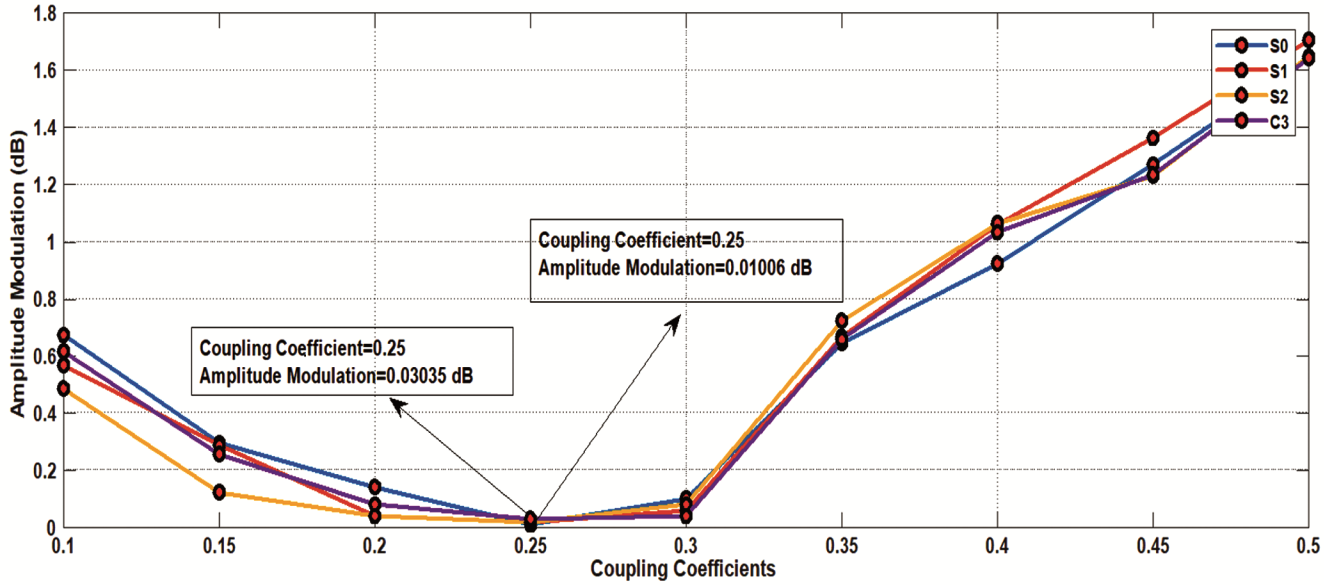

Fig. 18 — Deviations in the AM factor with various values of coupling coefficient

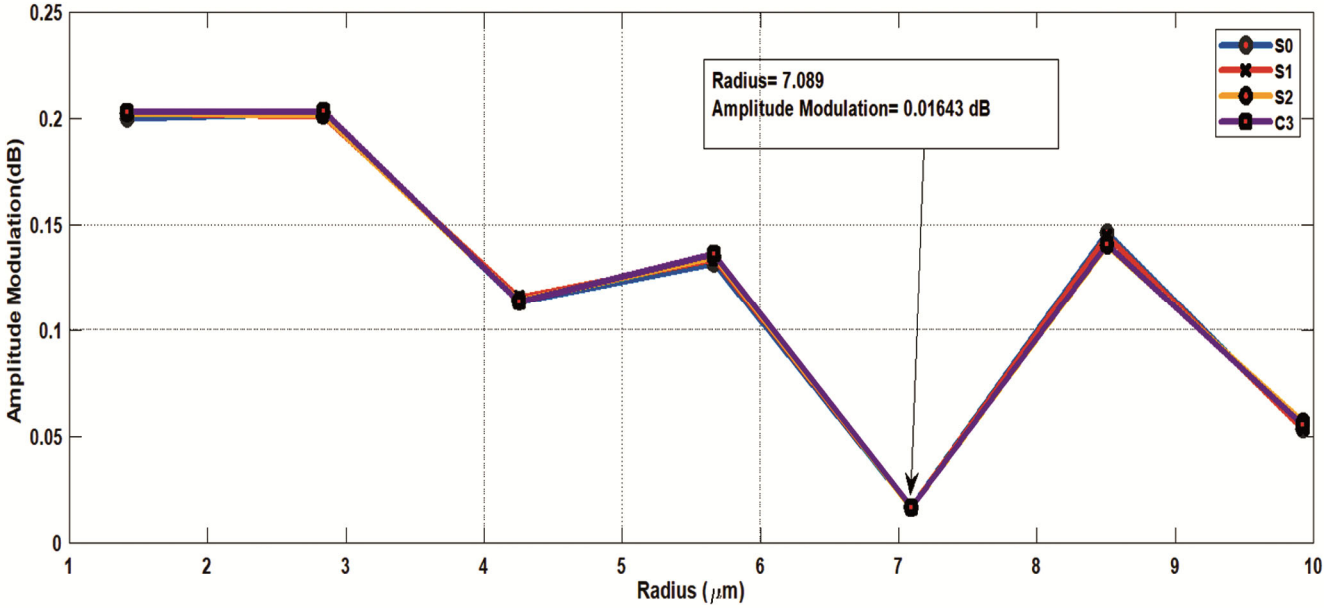

Fig. 19 — Deviations in the AM factor with various values of radius

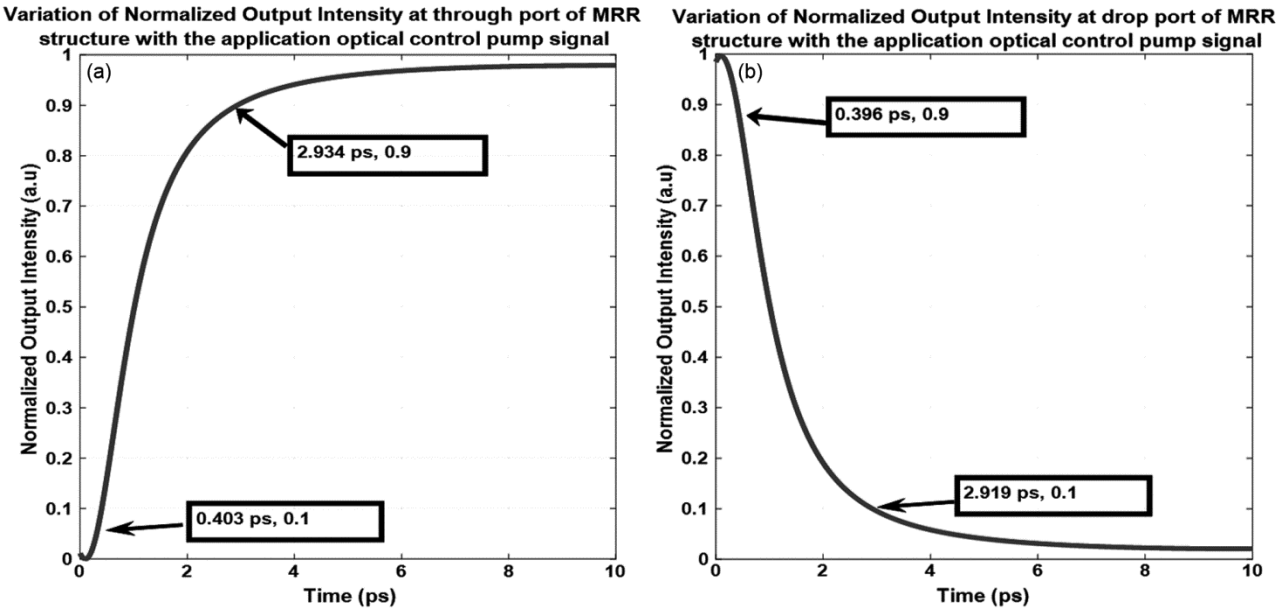

Fig. 20 — Switching Time Illustration (a) Rise Time (b) Fall Time

3 Conclusion

The work presents the design of an all-optical CLA adder circuit that uses MRR structures, indicating a prospective use in optical computing. The switching behavior of MRR constructs is explained in detail using mathematical models, emphasizing its potential in optical signal processing. The circuit's efficiency is maximized by thoroughly studying performance-affecting factors such as coupling coefficients and MRR radius. The proposed CLA adder circuit's architecture is designed to integrate an optimal arrangement of MRRs, as proven by simulated results that match conventional truth tables. Furthermore, the study emphasizes the larger implications of optical communication by presenting viable implementation options for digital circuits such as the CLA adder. Notably, characteristics like as extinction ratio, contrast ratio, amplitude modulation, and switching time are thoroughly explored in order to improve performance metrics. Finally, the described technique provides considerable benefits for integrated optical communication systems, such as reduced size, secure signal transfer, and higher bandwidth. The suggested approach has the potential to promote ultra-fast communication, particularly in the field of on-fiber integrated optics, making it promising for improving VLSIO applications.

References

1 Agrawal G P, *Nonlinear Science at the Dawn of the 21st Century*, Springer, Berlin, Heidelberg, (2000) 195.
2 Kumar A & Raghuwanshi S K, *Opt Quant Electron (Springer)*, 47 (2015) 2117.
3 Kumar A, Kumar S & Raghuwanshi S K, *Opt Commun (Elsevier)*, 324 (2014) 93.
4 Sribhashyam S, *et al*., *Int Conf Signal Process Commun Eng Syst, IEEE,* (2015).
5 Clavero R, *et al*., *IEEE Photon Technol Lett* 17 (2005) 843.
6 Yadav A, Kumar A & Prakash A, *J Electrical Eng*, 75 (2024) 14.
7 Kumar S, *et al*., *Appl Opt*, 54 (2015) 6397.
8 Yadav A, Kumar A & Prakash A, *Optik*, 288 (2023) 171190.
9 Saha S & Mukhopadhyay S, *Opt Laser Technol*, 131 (2020) 106386.
10 Murphy E J, Adda T F, Minford W J, Irwin R W, Ackerman E I & Adam S B, *IEEE Photon Technol Lett*, 8 (1996) 545.
11 Camargo E A, Chong H M H & Rue R M De La, *Opt Expr (OSA)*, 12 (2004) 588.
12 Law F K, Uddin M R, Hashim H & Hamid Z, *Opt Quant Electron*, 49 (2017) 413.
13 Kui L F & Uddin M R, *Opt Quant Electron (Springer)*, 49 (2017) 275.
14 Biswas U, *et al*., *Silicon*, 13 (2021) 885.
15 Rakshit J K, Chattopadhyay T & Roy J N, *Optik*, 124 (2013) 6048.
16 Zoiros K E, Papadopoulos G, Houbavlis T & Kanellos G T, *Opt Commun*, 258 (2006) 114.
17 Kumar A, *Opt Quant Electron (Springer)*, 48 (2016) 460.
18 Bharti G K & Rakshit J K, *Fiber Integr Opt*, (Taylor & Francis), 37 (2018) 103.
19 Kumar Ajay, Kumar M, Jindal S K & Raghuwanshi S K, *Opt Quant Electron*, (Springer Nature), 51 (2019) 191.
20 Rakshit J K & Roy J N, *Opt Appl*, 46 (2016) 517.
21 Bahadori M, *et al.*, *J Light Technol*, 36 (2018) 2767.
22 Mahanty S & Kumar A, *Braz J Phys*, 52 (2022) 69.
23 Rakshit J K, Roy J N & Chattopadhyay T, *J Comput Electron*, 13 (2014) 278.
24 Mahanty S & Ajay Kumar, *Opt Quant Electron*, 54 (2022) 601.

25 Rakshit J K, Zoiros K E & Bharti G K, *J Comput Electron*, 20 (2021) 353.
26 Sokoloff J P, *et al*., *IEEE Photon Technol Lett*, 5 (1993) 787.
27 Kumar A A, *Fundamentals of digital circuits*, PHI Learning Pvt Ltd, (2016).
28 Kumar K S K, Mahanty S, Kumar A, Kumari N, Shekhar S & Wagisha O, *3rd Int Conf Adv Electron Commun Eng (AECE)*, (2023) 401.
29 Mahanty S, Kumar A, Sharma U, Kumari S, Adhikary S & Pritam K A, *3rd Int Conf Adv Comput Commun, Embed Secure Syst (ACCESS),* (2023) 280.
30 Kundu S, Hossain M & Mandal S, *Opt Eng*, 63 (2024) 018102.
31 Hossain M, Mondal K, Kumar D, Rakshit J K & Mandal S, *Opt Quant Electron*, 55 (2023) 1100.
32 Chen F, Zhou S, Xia Y, Yu X, Liu J, Li F & Sui X, *Appl Opt*, 63 (2024) 147.